The polyadenylation landscape after *in vivo* long-term potentiation in the rat brain

Natalia Gumińska[1#], Francois P Pauzin[2,3#], Bożena Kuźniewska[4,5], Jacek Miłek[4,5], Patrycja Wardaszka[4,5], Paweł S. Krawczyk[1], Seweryn Mroczek[1,4], Sebastian Jeleń[1,5], Patrick U. Pagenhart[2], Clive R. Bramham[2,3*], Andrzej Dziembowski[1,4**] and Magdalena Dziembowska[4,5***]

[1] Laboratory of RNA Biology, International Institute of Molecular and Cell Biology, Warsaw, 02-109, Poland

[2] Department of Biomedicine, University of Bergen, Bergen, NO-5020, Norway

[3] Mohn Research Center for the Brain, University of Bergen, Bergen, NO-5020, Norway

[4] Faculty of Biology, University of Warsaw, Warsaw, 02-096, Poland

[5] Centre of New Technologies, University of Warsaw, Warsaw, 02-097, Poland

#equally contributed

*corresponding authors

Clive R. Bramham

mail: clive.bramham@uib.no

Andrzej Dziembowski

mail: adziembowski@iimcb.gov.pl

Magdalena Dziembowska

mail: m.dziembowska@uw.edu.pl

Running title

The poly(A) landscape after LTP in the rat brain

Abstract

Local protein synthesis in neurons is vital for synaptic plasticity, yet the regulatory mechanisms, particularly cytoplasmic polyadenylation, are not fully understood. This study employed nanopore sequencing to examine transcriptomic responses in rat hippocampi during *in vivo* long-term potentiation (LTP) and in synaptoneurosomes after *in vitro* stimulation. Our long-read transcriptomic dataset allows for detailed analysis of mRNA 3′-ends, poly(A) tail lengths, and composition. We observed dynamic shifts in polyadenylation site preference post-LTP

induction, with significant poly(A) tail lengthening restricted to transcriptionally induced mRNAs. Poly(A) tails of these genes showed increased non-adenosine abundance. In synaptoneurosomes, chemical stimulation led to shortening of poly(A) tails on preexisting mRNAs, indicating translation-induced deadenylation. Additionally, we discovered a group of neuronal transcripts with poly(A) tails abundant in non-adenosine residues. These tails are semi-templated and derived from extremely adenosine-rich 3′UTRs. This study provides a comprehensive overview of mRNA 3′-end dynamics during LTP, offering insights into post-transcriptional regulation in neuronal activation.

Introduction

Synaptic plasticity, the activity-dependent modification of synaptic efficacy, is critical for learning and memory processes (Citri & Malenka, 2008). It is divided into several paradigms, with the long-term potentiation (LTP) and long-term depression (LTD) being the primary models for synaptic strengthening and weakening, respectively. LTP has early and late phases, distinguished by their duration and underlying mechanisms. Early-phase LTP involves the activation of signal transduction pathways that modulate calcium-sensitive kinases. This enhances AMPA receptor conductance and leads to an increased number of AMPA receptors at the postsynaptic density (PSD) through exocytosis. Late-phase LTP, on the other hand, involves gene expression and *de novo* protein synthesis, which facilitate dendritic spine growth and PSD restructuring.

Pre-mRNA polyadenylation is a 3′-end processing mechanism for the export of RNAs from the nucleus into the cytoplasm. It contributes to mRNA stability and thus acts as a master regulator of gene expression in eukaryotes (Colgan & Manley, 1997). The polyadenosine tail, synthesized by the canonical poly(A) polymerase at the poly(A) site (PAS), is defined by upstream and downstream *cis*-regulatory elements recognized by the cleavage and polyadenylation specificity factor (Di Giammartino et al., 2011; Elkon et al., 2013; Fontes et al., 2017). Most mammalian genes contain multiple PASs, leading to multiple mRNA isoforms (Hoque et al., 2013). In neurons, local translation of mRNAs in dendrites and axons enables the rapid delivery of proteins involved in the regulation of synaptic maintenance, homeostasis and plasticity (Bramham & Wells, 2007). The interplay between alternative polyadenylation sites (APA) defining 3′UTRs, poly(A) tail length, translation, and mRNA decay is fundamental in gene expression regulation. Indeed, translational efficiency, as well as mRNA half-lives have been shown to vary more than 1,000-fold between individual transcripts, demonstrating the range and specificity of the regulation of mRNA stability and abundance (Eisen et al., 2020). Several

years ago, it was postulated that the translation of a specific group of mRNAs is activated by cytoplasmic polyadenylation (Du & Richter, 2005; Mansur et al., 2021). These transcripts have specific sequence motifs bound by CPEB proteins which initially induce deadenylation to store dormant mRNAs having short poly(A) tails. Upon stimulation, poly(A) tails are then extended to activate translation. In addition to polyadenylation, several other post-transcriptional regulatory mechanisms can regulate local protein synthesis including microRNAs or pathways that influence the activity of translation factors (Bramham et al., 2016; Cagnetta et al., 2023; Eisen et al., 2022; Jasińska et al., 2016; Thomas et al., 2018).

Despite the long-standing interest in poly(A) tails and the regulation of protein synthesis, methods for reliable, genome-wide estimation of poly(A) tail length have only recently been developed (Brouze et al., 2023). Initially, most studies relied on Illumina-based protocols, such as TAIL-seq and PAL-seq (Chang et al., 2014; Subtelny et al., 2014). However, DNA polymerase is unable to properly bind to long homopolymeric tracts (repetitive sequences) during PCR amplification, resulting in truncated estimates of poly(A) tail length. In addition, these methods require RNA fragmentation, as the sequencer can only read 200-300 base pairs at a time (Brouze et al., 2023).

Third-generation PacBio sequencing protocols, such as FLAMseq and PAIso-Seq, eliminate the upper limits of poly(A) tail length detection and provide a complete overview of the entire mRNA molecule (Legnini et al., 2019; Liu et al., 2019). However, they are still affected by amplification bias from library preparation, which calls into question the reliability of the results. Oxford Nanopore Technologies (ONT) offers a solution with its nanopore direct RNA sequencing (DRS) protocol. Unlike previous methods of poly(A) tail length measurement, DRS does not require amplification, allowing for real-time sequencing of single RNA molecules and generating full-length, strand-specific reads (Krause et al., 2019; Workman et al., 2019). This approach provides the most reliable poly(A) tail length estimations and, with our recently developed algorithm Ninetails (https://github.com/LRB-IIMCB/ninetails), can also analyze nucleotide composition (Gumińska et al., 2024). Additionally, long reads facilitate the study of other aspects of mRNA regulation, such as PASs usage (Pardo-Palacios et al., 2023).

Here we used nanopore DRS and cDNA sequencing to examine changes in expression and in poly(A) tail characteristics following LTP induction in the rat dentate gyrus *in vivo*. Our data provide first such a rich long-read transcriptomic resource and enables us to assess the dynamics of the 3′-ends of mRNAs during LTP. First, we have shown that a few genes are differentially expressed as early as 10 min after LTP induction, and that these changes are even more

pronounced 60 min post-LTP induction. While a few transcripts have an elongated poly(A) tail 10 min post-stimulation, a more prominent change was observed at 60 min, including both elongation and shortening. Second, we noticed a general tendency toward shortening of the 3′UTRs for both time points post-stimulation among all reported alternative polyadenylation events. Third, among the differentially expressed mRNAs, we observed an elevated proportion of poly(A) tails with non-adenosine residue insertions. We also found a specific group of neuronal mRNAs abundant in non-adenosines in their poly(A) tails. However, these possess extremely adenosine-rich 3′UTRs, suggesting that these tails are semi-templated. Finally, using the synaptoneurosome preparations, we show that the regulation of synaptic mRNA translation appears to be uncoupled from polyadenylation.

Results

Nanopore sequencing reveals expected changes in gene expression following LTP induction

To study the activity-induced changes in post-transcriptional regulatory programs in neurons, we used LTP in the rat dentate gyrus as an established *in vivo* model for synaptic plasticity. Short bursts of high-frequency stimulation (HFS) were applied to one hemisphere (ipsilateral DG), while the unstimulated hemisphere (contralateral DG) served as a control (Figure 1A). HFS of the medial perforant path input to DG (Figure 1B) resulted in a rapid and stable potentiation of the field excitatory postsynaptic potential (fEPSP) slope: 57+/-13% for 10 min and 55+/-7% for 60 min (Figure 1C). The increase in the fEPSP slope is accompanied by a rise in population spike amplitude (Figure 1C insert). Then, after *in vivo* LTP induction (10 and 60 min), both ipsi- and contralateral dentate gyri were dissected for RNA extraction. Since successful LTP induction leads to the expression of immediate early genes (IEGs) such as *Arc* and *Fos* (Chen et al., 2017; Demmer et al., 1993; Guzowski et al., 1999; Kim et al., 2018; Maag et al., 2015; Patil et al., 2023), we only analyzed the samples with increased expression of these markers in the ipsilateral hemisphere (Supplementary Figure 1).

To investigate the transcriptomic changes induced by neuronal activity after *in vivo* HFS, we applied two different nanopore sequencing approaches: Nanopore Direct RNA Sequencing (DRS) and Nanopore cDNA from Oxford Nanopore Technologies (ONT). Both methods produce reads that encompass whole molecules of interest, overcoming the limitations of Illumina (Pardo-Palacios et al., 2023). In particular, DRS provides insights into the mRNA inventory without a synthetic proxy, avoiding amplification bias (Brouze et al., 2023; Workman et al., 2019), whereas cDNA sequencing yields higher coverage, ensuring that sufficient data is

available for less expressed genes (Sessegolo et al., 2019; Wongsurawat et al., 2022). With DRS, we obtained an average of 0.5 million reads per sample/run, while with cDNA sequencing we obtained about 15 million reads per sample/run, which met the requirements of the analysis. DRS on ipsi- and contralateral dentate gyri confirmed HFS-dependent induction of IEGs (including *Arc* and *Fos* as well as many others) in agreement with the qPCR data (Figure 1D; Supplementary Figure 1). The 10 min post-HFS time point was chosen because we wanted to compare the mRNA polyadenylation status before induction of gene expression. However, we found 59 and 57 induced transcripts at 10 min post-HFS using DRS and cDNA sequencing, respectively (Figure 1E, left panels). We did not identify any significantly downregulated transcripts at 10 min. 60 min post-HFS showed more prominent changes in gene expression than the 10 min post-HFS: 127 and 188 transcripts were significantly differentially expressed using DRS and cDNA sequencing, respectively (Figure 1E, right panels). The overlap between the two methods is substantial: 60% of the differentially expressed genes (DEGs) identified by DRS at 10 min were confirmed by cDNA sequencing, and at 60 min it was even over 80% (Figure 1E, F, Supplementary Table 1, Supplementary Table 2).

Numerous specific regulatory motifs reside within mRNA sequences, predominantly in the 3′UTRs. These elements are targets for mRNA-contacting ribonucleoprotein molecules or proteins. Among them, CPEB proteins play important regulatory roles in affecting the dynamics of poly(A) tails (de Moor & Richter, 1999; McFleder et al., 2017). Therefore, we investigated the presence of a CPEB-binding motif in the DEGs. Indeed, a significant fraction of upregulated transcripts harbor CPEB-binding sites (Figure 1E, F; see also Figure 2A, 3B).

We conclude that LTP-inducing stimulation *in vivo* leads to the expected changes in gene expression as determined by both DRS and cDNA long-read sequencing, providing a basis for a detailed survey of the mRNA 3′-ends and poly(A) tails.

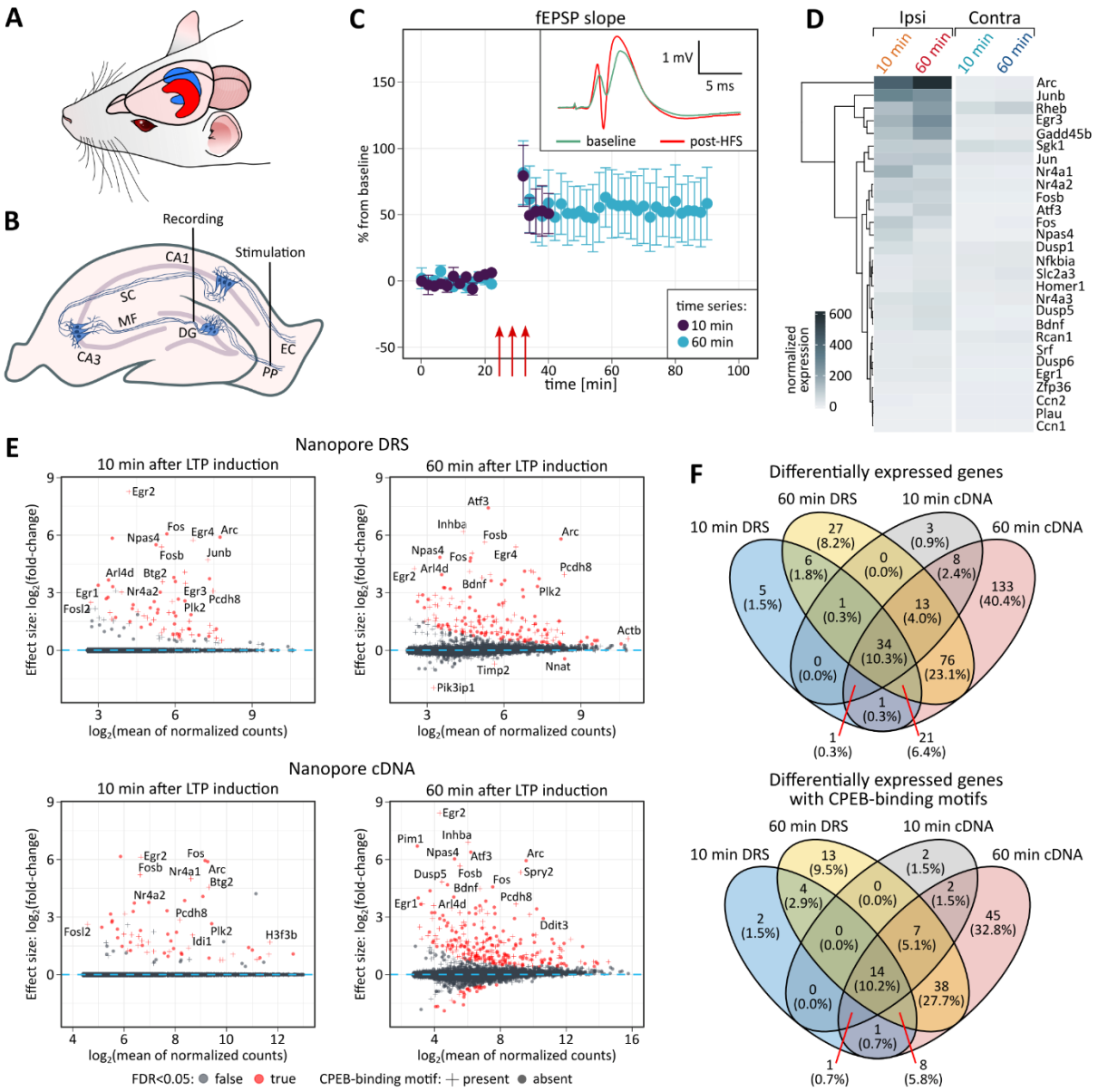

Figure 1. *In vivo* hippocampal LTP induction. (A) Schematic depiction of dentate gyrus with LTP-induction (left hemisphere, ipsilateral) marked in red and control dentate gyrus (right hemisphere, contralateral) marked in blue. (B) Schematic coronal section of the hippocampus with stimulating and recording electrodes positions; DG – dentate gyrus, MF – mossy fibers, SC – Schaffer collateral, PP – perforant path, EC – entorhinal cortex. (C) Representative recordings of HFS-induced LTP in anesthetized rats. Time course plots of percent change in fEPSP slope post-HFS (10 min and 60 min after HFS) relative to baseline. Values are mean ± SEM. Red arrows represent three sessions of HFS. Insert: Representative traces before (baseline, green) and after HFS (post-HFS, red. (D) Expression levels of selected IEGs induced in the dentate gyrus following LTP (Ipsi) as compared to control (Contra). Colors indicate normalized expression values as shown by the scale on the left (log2 change). (E) DEGs in the rat dentate gyrus after *in vivo* LTP induction. The expression changes ($\log_2$ ratios) 10 min (left panels) and 60 min (right panels) after HFS. DEGs are colored in red. Genes containing CPEB-binding motifs are marked as crosshair (+), genes lacking CPEB-binding motifs are marked as dots. Results obtained with two Nanopore methods: Direct RNA sequencing (DRS) (top panels) and cDNA sequencing (bottom panels) are shown. (F) The overlap between differentially expressed genes 10 min and 60 min after LTP induction using both DRS and cDNA.

Dynamics of mRNA poly(A) tail lengths following LTP induction

Next, we investigated poly(A) tail dynamics following activity-dependent synaptic plasticity using the DRS and cDNA-seq datasets.

Indeed, we observed changes in the distribution of poly(A) tail lengths, with a gradual increase in a subset of transcripts affected upon LTP (Figure 2A). Initially, 10 min post-HFS, a significant change of tail length occurred in 54 genes, of which 44 underwent tail extension. The Cohen's d effect size of this elongation was medium for ten genes (*Nrn1, Egr3, Sat1, Vgf, Dstnl1, Arpp21, Egr1, Fosl2, Ddit3 and Spns2*; with a mean tail length difference between ipsi- and contralateral hemispheres of 42.3 nt), small for 27 (e.g. *Actb*, *Nefl*, *Dnaja1*, *Nefm*, *Nptx1*, *Dclk1I;* with a mean tail length difference between ipsi-and contralateral hemispheres of 20.0 nt), and negligible for 4 genes (*Tuba1a*, *Ckb*, *Enc1*, *Hsp90aa1*; with a mean tail length difference between ipsi-and contralateral hemispheres of 7.59 nt). Among them, the most significantly enriched GO-terms were associated with synapse organization, activity, and transport (Supplementary Figure 2). In contrast, 60 min post-HFS, a significant change in tail length occurred in 417 genes, 74 of which were elongated. The size of this effect was large for 8 genes (*Baiap2*, *Arpp21*, *Homer1*, *Nrbf2*, *Jarid2*, *Plekha2*, *Htra4*, *Mob3a*; with a mean tail length difference between ipsi-and contralateral hemispheres of 74.38 nt), medium for 22 genes (e.g. *Nrn1*, *Rheb*, *Vgf*, *Rtn4rl2*, *Egr3*, *Rbbp7*, *Synpo* and *Penk*; with a mean tail length difference between ipsi-and contralateral hemispheres of 45.64 nt), small for 40 genes (e.g. *Nefl*, *Dnaja1*, *Nefm*, *Nptx2*, *Dclk1*, *Nrp1* and *Stmn4*; with a mean tail length difference between ipsi-and contralateral hemispheres of 21.5 nt) and negligible for 4 genes (*Actb*, *Rpl41*, *Nptx1* and *Tubb4b*; with a mean tail length difference between ipsi-and contralateral hemispheres of 8.94 nt). The most enriched GO-terms were linked to cell projection and synapse organization, protein trafficking, and neurodevelopment (Supplementary Figure 2).

We then compared changes in mRNA expression with changes in average tail length to analyze whether they correlate (Figure 2B). At both time points, we observed accumulation of certain mRNAs (e.g., *Nefl*, *Nrn1*, *Baiap2*, *Homer1*), including known IEGs (e.g., *Egf3*, *Nr4a1*) with elongated poly(A) tails. Simultaneously, a large number of mRNAs with shortened poly(A) tails at the 60 min time point correlated with their downregulation. All this suggests that poly(A) tail extension is driven by transcriptional induction and nuclear 3′-end formation rather than local cytoplasmic processes. Downregulated mRNAs are at the same time undergoing deadenylation-dependent decay manifested by shortened poly(A) tails. Deadenylation is likely to accelerate because *Btg2*, a general deadenylation activator, is among the IEGs induced by the HFS (see Figure 1E) (Mauxion et al., 2008). We also detected a handful of transcripts in

which the elongation of poly(A) tail was independent of gene expression upregulation. Those included *Enc1* and *ActB*.

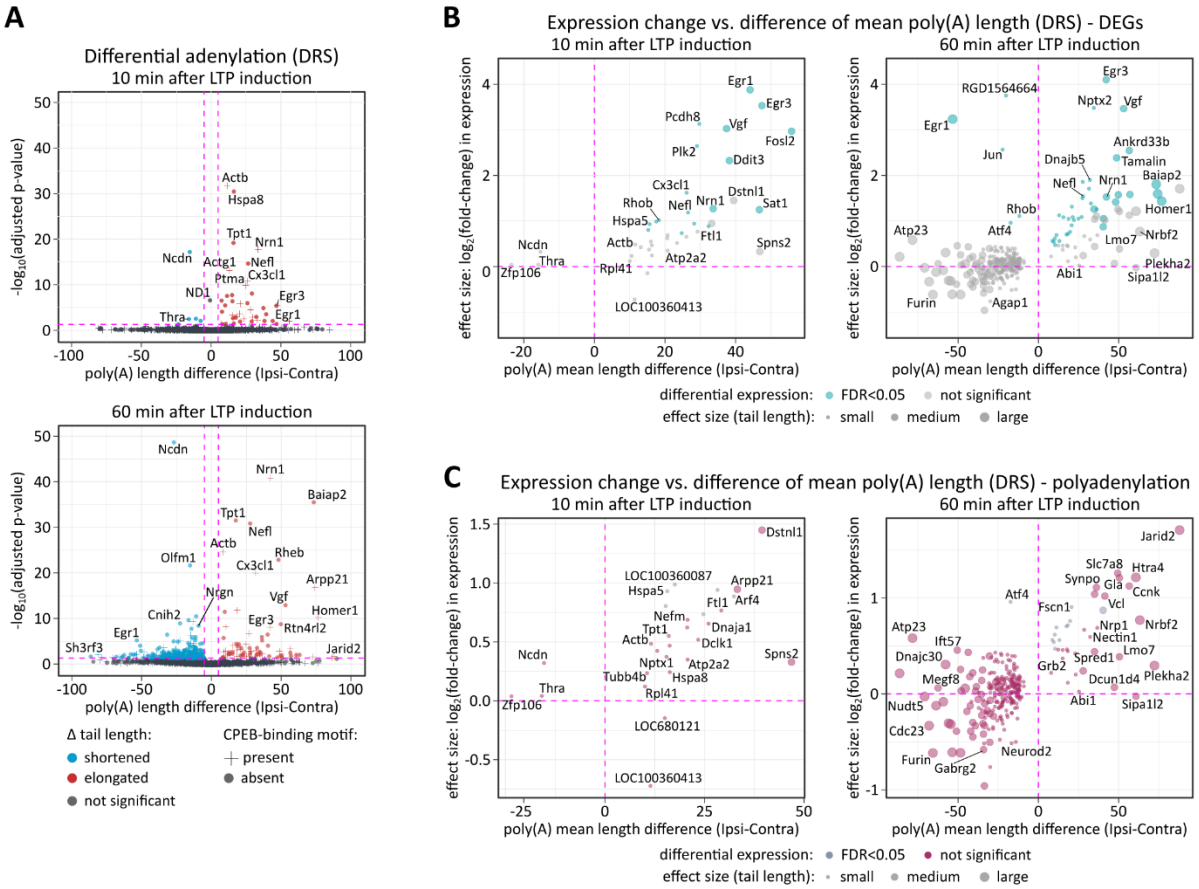

Figure 2. Dynamics of mRNA poly(A) tail lengths following LTP induction. (A) Poly(A) tail length changes 10 min and 60 min after HFS. (B) Differential expression vs differential polyadenylation for 10 min post-HFS and 60 min post-HFS. Genes with significantly changed expression and poly(A) length are highlighted (teal). (C) Differential expression vs differential polyadenylation for 10 min post-HFS and 60 min post-HFS. Genes with unchanged expression and significantly changed poly(A) length are highlighted (fuchsia). (D) Distribution of poly(A) lengths in selected transcripts across experimental conditions.

Since mRNAs bound by CPEB proteins are predicted to be the major targets of cytoplasmic poly(A) tail lengthening, we then narrowed our investigation to transcripts containing CPEB motifs (CPEB1 and CPEP2,4) and compared them with the overall changes in poly(A) tail length distribution (Huang et al., 2023) (Figure 3A, B). In general, the presence of CPEB-binding motifs did not correlate with poly(A) length distribution. Elongation was only observed on DEGs with the strongest effect on mRNAs with CPEB1-binding motif 10 min post-LTP (Figure 3B, Supplementary Figure 2).

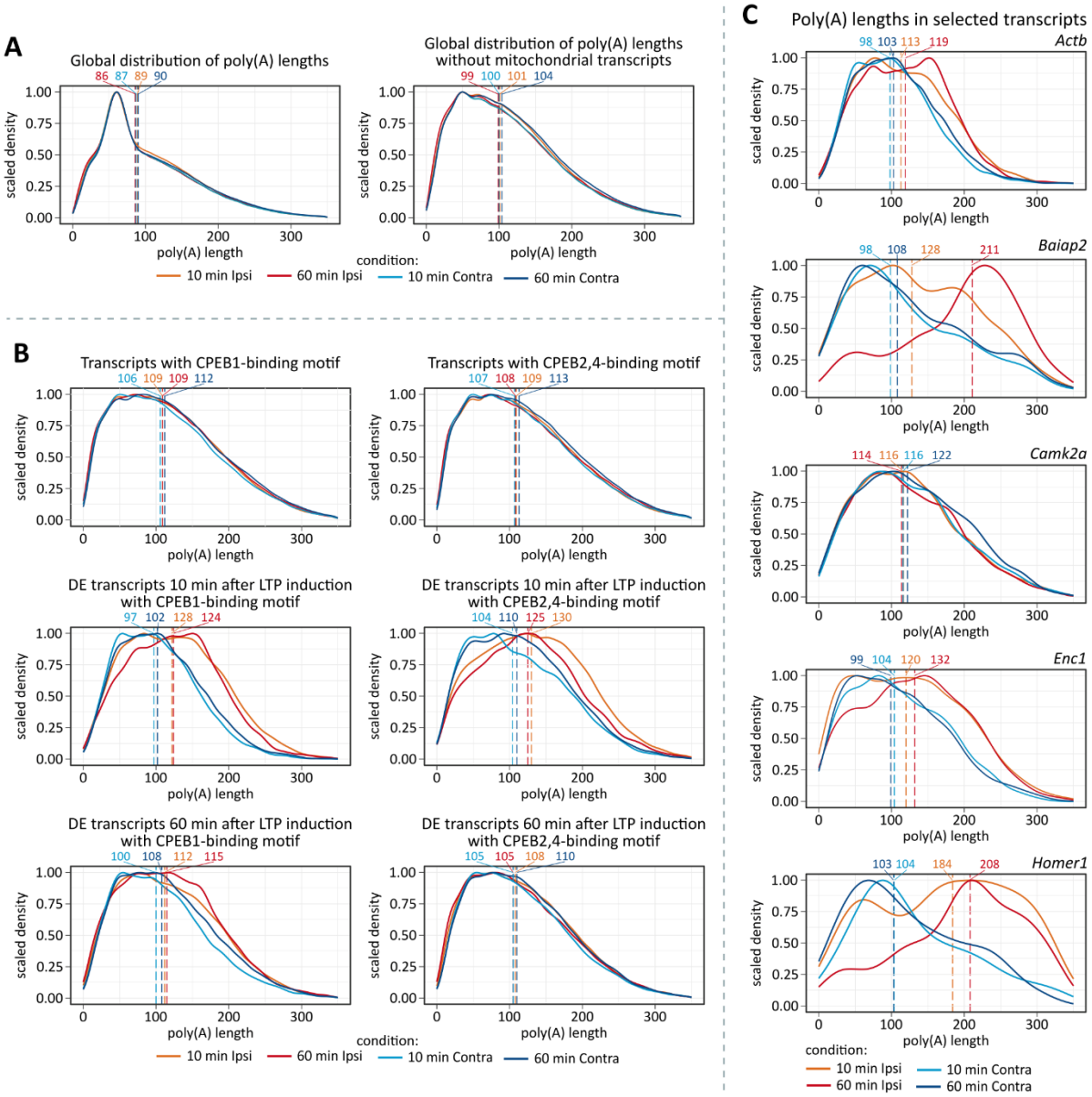

Figure 3. Distribution of poly(A) lengths in selected groups of mRNAs. (A) Global distribution of poly(A) lengths: upper panel – complete datasets, bottom panel – global distribution without mitochondrially-encoded genes. (B) Distribution of poly(A) lengths in CPEB-targets. Upper left: transcripts with CPEB1-binding motifs (total). Upper right: transcripts with CPEB2,4-binding motifs (total). Middle left: transcripts with CPEB1-binding motifs which were differentially expressed 10 min after LTP induction. Middle right: transcripts with CPEB1-binding motifs which were differentially expressed 60 min after LTP induction. Bottom left: transcripts with CPEB2,4-binding motifs which were differentially expressed 10 min after stimulation. Upper right: transcripts with CPEB2,4-binding motifs which were differentially expressed 60 min after LTP induction. In each panel, all conditions were included.

Ultimately, we examined specific transcripts recognized for their significant role in hippocampal synaptic plasticity (Figure 3C). Yet again, we did not see signs of cytoplasmic polyadenylation in our data. Notably, this was also the case for *Camk2a* ($Ca2^{+}$/calmodulin-dependent protein kinase 2), acknowledged for its activity-dependent polyadenylation (Figure

3C) (Du & Richter, 2005; L. Wu et al., 1998). This unexpected outcome may be attributed to the relatively lower coverage provided by DRS compared to amplification-based methods. Therefore, we corroborated our findings with our cDNA data. Noteworthy, DRS and cDNA turned out to be fully consistent in estimating tail length distributions (Supplementary Figure 3).

These findings demonstrate that the poly(A) tail length of certain mRNAs increases as a result of polyadenylation of the nascent mRNAs. Furthermore, none of the mRNAs with elongated tails exhibited a significant reduction in accumulation or a detectable decrease in short-tailed read abundance, which corresponds with previous studies (Eisen et al., 2022).

Several mRNAs feature LTP-induced changes in APA site usage

Most mammalian genes contain multiple polyadenylation sites located predominantly within the 3′UTR region of the mRNA (Figure 4A). Because 3′UTRs often contain binding motifs for RNA-binding proteins and miRNA target sites, alterations in their length present an efficient method for regulating gene expression. Alternative polyadenylation (APA) site usage is another post-transcriptional mechanism postulated to be pivotal in LTP (Fontes et al., 2017). Therefore, we sought to explore whether and how alternative polyadenylation site usage is changed after *in vivo* LTP induction in the rat brain (Arora et al., 2021; Ha et al., 2021). To examine APA profiles following LTP induction, we investigated cDNA reads. Since cDNA sequencing was considerably deeper than DRS, more accurate profiling could be achieved. First, to ensure that the cDNA data was free of nanopore systemic errors (e.g. fused reads), the datasets were curated using pychopper. Subsequently, we applied TAPAS, a software for detecting APA events in sequencing data (Arefeen et al., 2018).

With TAPAS, we identified over 19,000 unique polyadenylation sites (PASs) in more than 13,500 genes, of which over 3,500 (~30%) contained at least two PASs, without significant difference in the number of PASs per gene between LTP and control samples (Figure 4B). Motif enrichment analyses of sequences around PASs confirmed the significant overrepresentation of hexamer motif A[U/A]UAAA and its variants approximately 20 nt upstream of PASs (Figure 4C). Results were comparable for both control and LTP samples 10 min and 60 min post-HFS, and they were in agreement with previous studies (Fontes et al., 2017; Wang et al., 2022).

Most of the identified PASs were already known. Nearly half of these were found in the 3'UTRs, ~10% within transcripts (including introns), and ~3% in exons. Notably, however, more than 30% of detected PASs were identified as intergenic (i.e. located outside 3'UTR in the reference

annotation). Therefore, these are novel isoforms equipped with long UTRs, consistent with numerous reports demonstrating that in the nervous system, UTRs are longer than in other tissues (Miura et al., 2013; Tushev et al., 2018) (Figure 4D). We then corrected and supplemented the predictions from TAPAS with another tool, LAPA (Çelik & Mortazavi, 2022). In such a way, we generated a resource of a high-confidence set of PASs clusters, which is a comprehensive annotation of 3′UTRs and PASs of rat brain transcripts, including previously unreported PASs (Supplementary Resource).

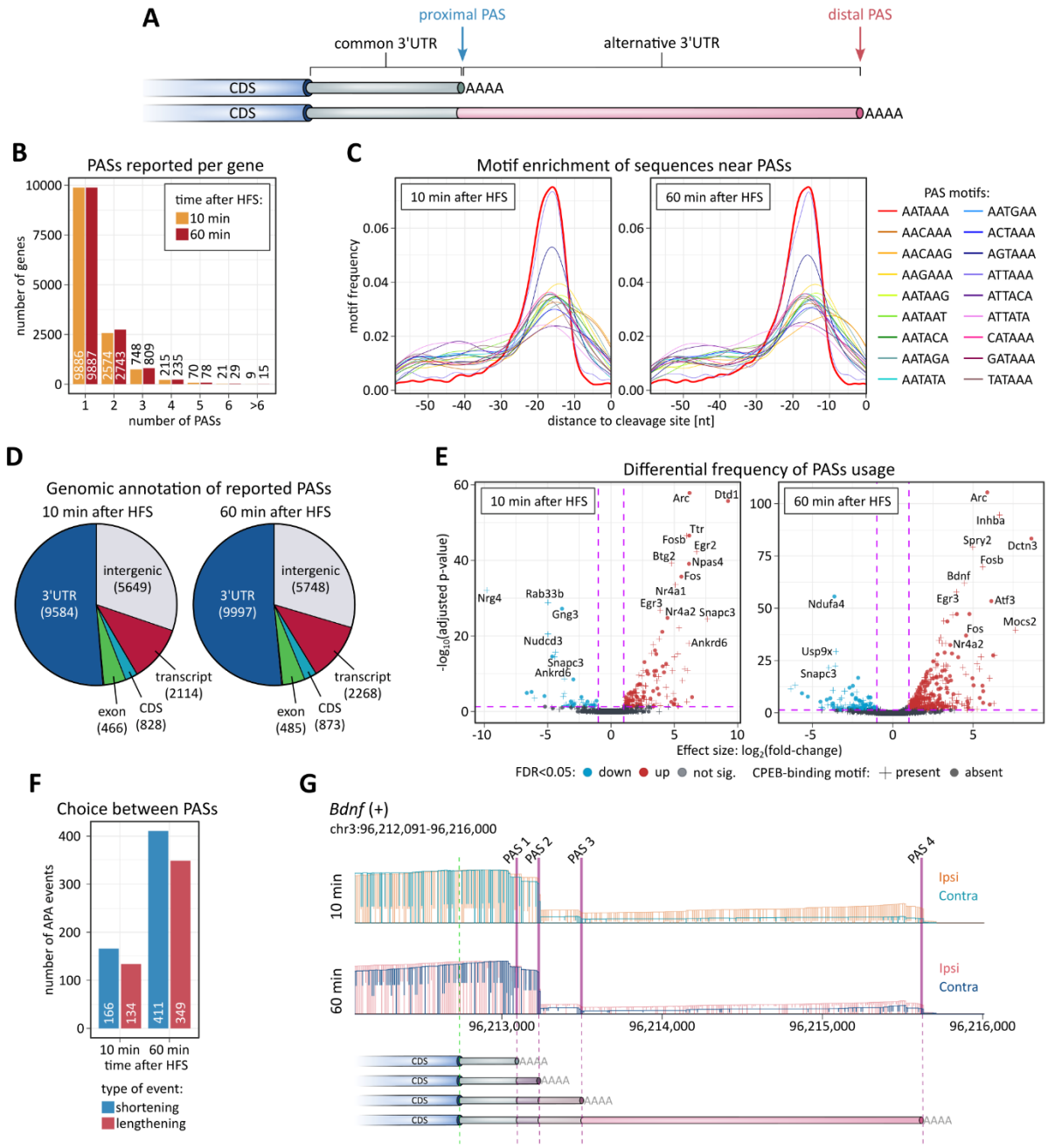

Figure 4. Differential polyadenylation site usage. (A) Schematic depiction of 3′UTR containing multiple PASs. (B) Number of PASs per gene reported by TAPAS. (C) Enriched motifs near detected PASs. (D) Genomic location assignment of reported PASs. (E) Relationship between PASs usage and expression level. (F) Usage of distal and

proximal PASs in genes with at least two PASs reported. (G) An example of a gene associated with neuroplasticity (*Bdnf*) exploiting multiple PASs with differential frequency. A genome browser-like view of coverages in 3′UTR region across conditions is shown.

Next, we analyzed 3′UTR APA events and determined whether the length of 3′UTR was changed globally following LTP induction. In the total number of 9228 high-confidence genes, we identified 186 differentially used PASs in 174 genes 10 min after LTP induction and 556 differentially used PASs in 480 genes 60 min post-HFS (Figure 4E). A common set of 115 genes changing expression between time points included immediate early genes, such as *Arc*, *Fos*, *Jun*, *Btg2*, *Bdnf*. According to the GO term analysis, genes with differentially used PASs were enriched in cognition, learning and memory 10 min after HFS, and rhythmic processes, regulation of phosphorus/phosphate metabolic processes and axonogenesis 60 min after LTP induction (Supplementary Figure 4). *Bdnf* is an example of activity-regulated mRNA with multiple APA sites (Lau et al., 2010). Here, we show that 10 min post-HFS, the isoform of *Bdnf* mRNA with longer 3′UTR is more abundant, whereas 60 min post-HFS, isoform with short 3'UTR is predominant.

Notably, we observed a strong link between LTP-induced changes in PAS usage and LTP-induced changes in transcript abundance (Figure 4E, compare to Figure 1E). Furthermore, among all reported APA events, we noticed a general tendency to shorten the 3′UTRs, regardless of time point (Figure 3F), suggesting that proximal PASs are favored.

Neuronal mRNAs with semi-templated poly(A) tails rich in non-adenosine residues

We then examined the nucleotide composition of poly(A) tails in DRS reads using our recently developed software, Ninetails (Gumińska et al., 2024). Remarkably, in data from both hemispheres (10 and 60 min post-HFS and in corresponding controls), we observed a fraction of tails containing non-adenosines (Figure 5A), mostly found only one instance of non-adenosine per tail, rarely two or more, coherent with our recent data (Figure 5B) (Gumińska et al., 2024; Legnini et al., 2019). The global proportion of decorated tails was relatively low, slightly above 3%, remaining stable across the conditions (Figure 5A). Subsequently, we focused on certain groups of reads: mitochondrial, DEGs 10 min post-HFS, DEGs 60 min post-HFS and potential CPEB targets. In our recent study, we found that mitochondrial transcripts have short but highly decorated tails, reflecting various fidelities of the cellular poly(A) polymerases (Gumińska et al., 2024; Lim et al., 2018). Here, in data from both hemispheres, the proportion of decorated tails in mitochondrial transcripts was also relatively high and nearly equivalent to the total. It also remained relatively constant, as the distribution of their tail

lengths (Figure 5A). Conversely, in both DEGs subsets and in transcripts containing CPE motifs, we observed an elevated proportion of decorated reads following LTP induction compared to the corresponding controls (Figure 5A). This can be attributed to the activation of transcriptional mechanisms leading to the synthesis of new molecules with longer tails, wherein polymerase-induced errors are more likely (Gumińska et al., 2024).

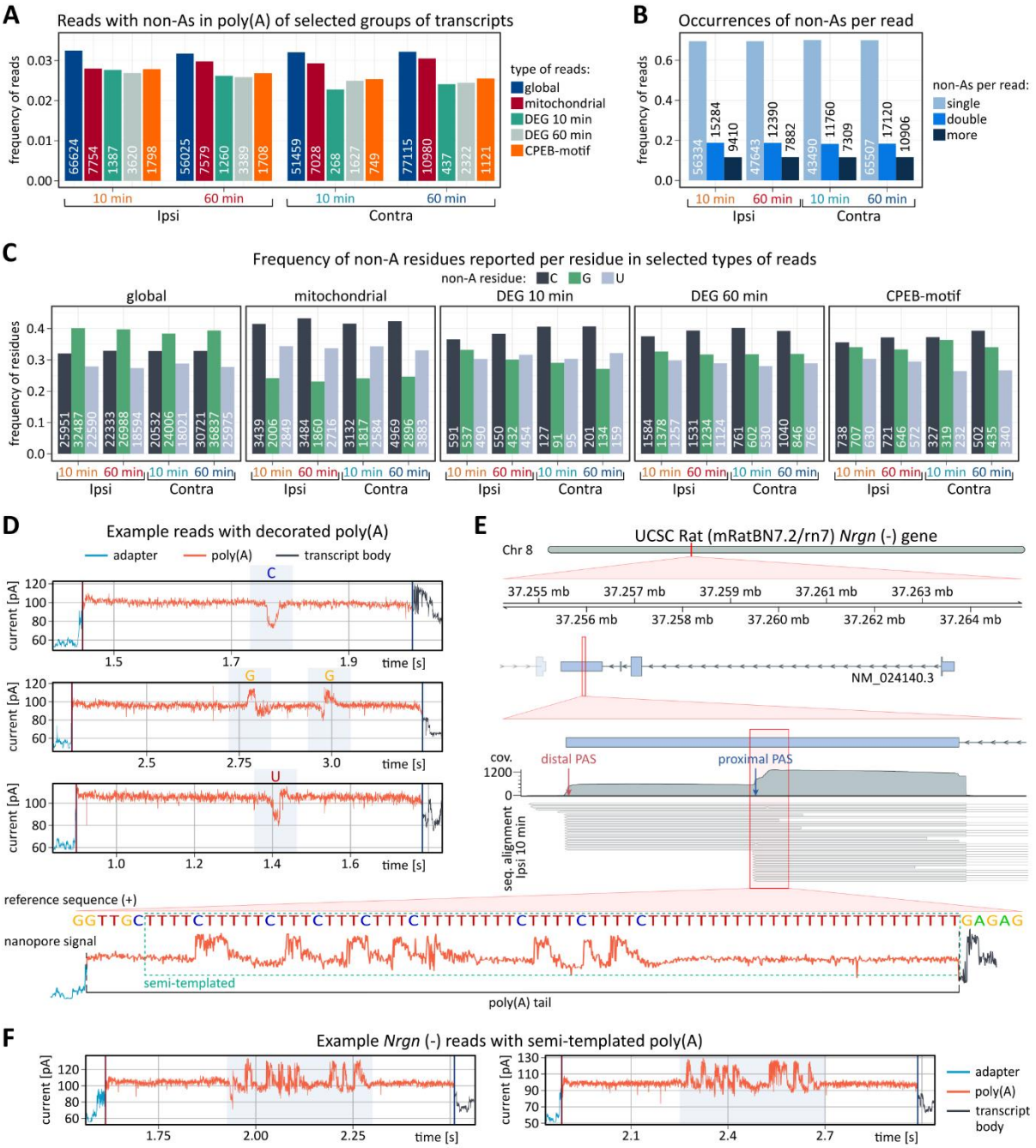

Figure 5. Non-adenosine residues in poly(A) tails; Neurogranin as an example of semi-templated poly(A) tails with increased frequency of non-adenosine residues. (A) Frequency of reads with poly(A) tails decorated with non-adenosines. Data normalized on y-axis (each group separately). (B) Frequencies of decorated reads with a given number of non-adenosines. (C) Frequency of non-adenosine residues (cytidine, guanosine, and uridine, respectively) in selected groups of reads: total datasets, mitochondrially-encoded genes, DEGs (each time point

separately) and in CPEB targets (aggregated). (D) Example nanopore signals corresponding to decorated tails. Non-adenosine residues reported by Ninetails are shown. (E) Genome-browser plot of reads aligned to 3'UTR of *Nrgn* gene with an example of corresponding nanopore signal revealing semi-templated poly(A) tail origin in isoform using proximal PAS and internal non-adenosines (guanosines) in fixed positions. (F) Example nanopore signals corresponding to semi-templated tails of Nrgn isoform with shorter 3′UTR. Non-adenosine residues (guanosines) in fixed positions reported by Ninetails are shown.

We also noticed that non-adenosines are more common in longer tails (Supplementary Figure 5A), suggesting that they are inserted late by terminal nucleotidyltransferases (TENTs) in the cytoplasm (Lim et al., 2018; Warkocki et al., 2018; Yu & Kim, 2020). The obvious candidates are TENT4A/B known for their incorporation of non-adenosines (Supplementary Figure 5B) (Lim et al., 2018; Warkocki et al., 2018; Wen et al., 2023; Yu & Kim, 2020), which is supported by the fact that at the global level guanosine is most prevalent, followed by cytidine and uridine (Figure 5C, D), This contrasts with other experimental systems, where cytidine is the most common and guanosine the least common (Gumińska et al., 2024; Legnini et al., 2019). Notably, gene level analysis followed by closer inspection of Ninetails output and raw nanopore signals unveiled a subset of transcripts with tails significantly enriched in non-adenosines. The most notable example is the *Nrgn* gene, where nearly 60% of the tails were decorated with (often multiple) guanosines (Figure 5D, E, F). According to APA analysis results, *Nrgn* has two PASs (Supplementary Resource, Supplementary table 3). Reads utilizing the distal PAS have blank tails (i.e. containing exclusively adenosines), whereas reads using the proximal PAS have highly decorated tails with a strikingly repetitive non-adenosine distribution pattern (Figure 5E, F). Further analysis revealed that this regularity is due to the semi-templated tail, as in this isoform the short genomically encoded 3′UTR has an extremely A-rich 3′-end directly followed by poly(A) (Figure 5E, F). In total, we identified 54 genes (e.g., *Grin2b*, *Kalrn*, and *Shank1*) whose transcripts may possess such semi-templated tails (Supplementary Table 4), which is the source of high guanosine prevalence rather than TENT4A/B activity. Interestingly, the most enriched GO-terms assigned to them were associated with learning, neuron reorganization, memory, and regulation of LTP (Supplementary Figure 5C), suggesting the potential regulatory role of such a newly described group of transcripts.

In the synaptic compartment, the polyadenylation is not induced by NMDA-R stimulation *in vitro*

Potential cytoplasmic polyadenylation in our hippocampal data might have been obscured by highly expressed transcripts from non-neuronal cells or by the predominant effect of transcriptional induction (i.e., the influx of newly synthesized long-tailed molecules) (Eisen et al., 2022). Unable to indicate transcripts undergoing local polyadenylation in the whole dentate

gyrus in response to HFS, we chose a more specific setup: synaptoneurosomes stimulated chemically *in vitro* (Figure 6A) (for details see Methods) (Kuzniewska et al., 2018, 2020). Enrichment and stimulation of synaptoneurosomes were performed using our optimized protocol, which effectively activates translation, leading to *de novo* protein synthesis (Kuzniewska et al., 2018, 2020). The effectiveness of this protocol can be confirmed by western-blots (e.g. depletion/enrichment of specific markers and phosphorylation of ERK kinases) (Supplementary Figure 6A, B).

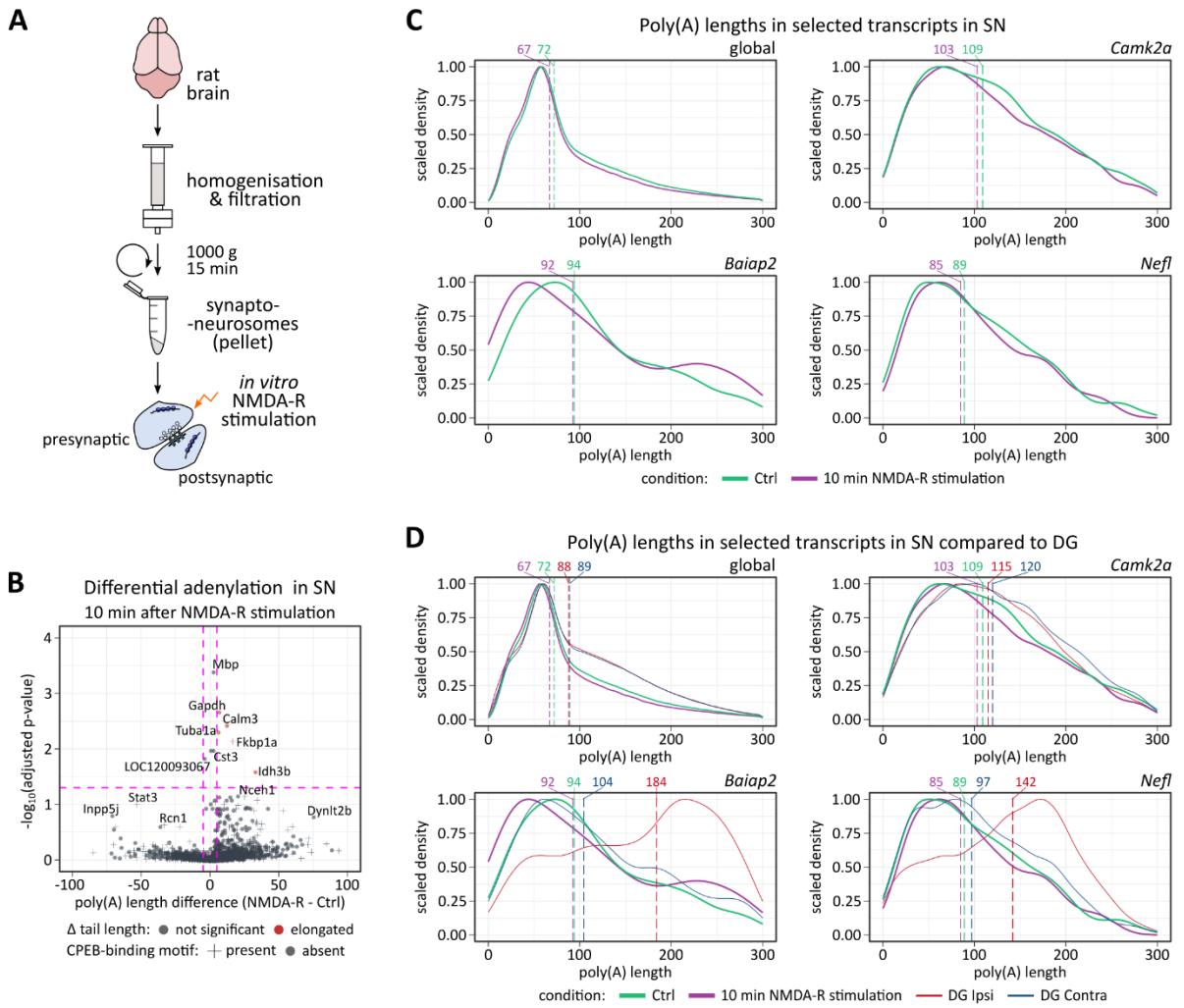

Figure 6. Poly(A) tail length distribution in synaptoneurosomes 10 min after *in vitro* NMDA-R stimulation. (A) Schematic depiction of synaptoneurosomes isolation and *in vitro* stimulation. (B) Polyadenylation profile of mRNAs in synaptoneurosomes upon NMDA-R stimulation. (C) Poly(A) tail length distribution in selected groups of transcripts in synaptoneurosomes. Upper left: global (total datasets). Upper right, bottom left, and bottom right, respectively: *Camk2a*, *Baiap2*, and *Nefl* – genes related to synaptic plasticity. (D) Poly(A) tail length distribution in selected groups of transcripts in synaptoneurosomes vs dentate gyrus. The data from the given hemisphere in dentate gyrus were aggregated across time points for clarity.

We performed DRS of mRNAs isolated from NMDA-R-stimulated synaptoneurosomes and corresponding controls to gain an accurate view of extranuclear polyadenylation (4 replicates).

As expected, we did not observe differences in transcript abundance between the conditions (Supplementary table 5). However, the polyadenylation profile also was largely unchanged (Figure 6B). Specifically, no shift of putative dormant transcripts towards longer tails was noted in stimulated synaptoneurosomes (Eisen et al., 2020, 2022). Instead, we observed a very small fraction of oligoadenylated mRNAs and general slight shortening poly(A) tail lengths compared to controls. Analyzing poly(A) tail length distribution in transcripts related to synaptic plasticity also failed to confirm local cytoplasmic polyadenylation upon stimulation (Figure 6C). There were also fewer non-adenosines in stimulated synaptoneurosomes than in corresponding controls (Supplementary Figure 6C-E).

Finally, when the poly(A) tail distribution of the synaptoneurosomes and total RNA of dentate gyri was compared, the former ones exhibited considerably shorter poly(A) tails (Figure 6D).

In conclusion, synaptic mRNA translation regulation appears uncoupled from polyadenylation.

Discussion

Local protein synthesis at synapses is regulated by several post-transcriptional mechanisms, which is necessary given the distance of synapses from the nucleus-containing cell body. Because of this spatial separation, rapid, on-demand protein synthesis relies on translational rather than transcriptional mRNA regulation. This is evident even in simple *in vitro* systems, where isolated synaptic fractions, when chemically induced, show substantial global activation of protein synthesis (Kuzniewska et al., 2018, 2020). Such observations emphasize the role of translation over transcription in these situations.

In our study, we complemented *in vivo* long-term potentiation (LTP) in the rat hippocampus with *in vitro* synaptoneurosomes and applied long-read sequencing technologies: direct RNA and cDNA sequencing. This allowed us to make an unbiased assessment of poly(A) tail dynamics and mRNA 3′-ends, providing valuable resources on APA site usage, tail length distribution, and its nucleotide composition after neuronal stimulation.

It has been postulated that cytoplasmic polyadenylation plays a central role in regulation of translation at synapses (Huang et al., 2023). This mechanism, originally observed in developing oocytes and early embryos (Richter, 2007), involves dormant mRNAs with short poly(A) tails that are elongated upon activation by cytoplasmic poly(A) polymerases, rapidly initiating protein synthesis. RNA-binding proteins, in particular the CPEB family, are thought to be key regulators of this polyadenylation process. Interestingly, recent studies suggest that not only the length but also the composition of poly(A) tails influences gene regulation (Yu & Kim, 2020).

Surprisingly, our results did not indicate robust cytoplasmic polyadenylation in the hippocampus, challenging the previously understood role of this mechanism in neuronal function. This raises the question of the physiological role of the relatively abundant GLD2/TENT2 poly(A) polymerase, which was previously hypothesized to be responsible for CPEB-regulated cytoplasmic polyadenylation (Mansur et al., 2016; Udagawa et al., 2012). At the same time, members of another family of cytoplasmic poly(A) polymerases, TENT5, have very low expression in the hippocampus. The remaining two polymerases, TENT4A and TENT4B (GLD4), are known to incorporate guanosines into poly(A) tails (Lim et al., 2018), and this nucleotide is most abundant in hippocampal mRNAs compared to cyidines and uridines. However, the guanosines are present in less than 4% of the poly(A) tails of hippocampal mRNAs, with the exception of mRNAs described by our group as having semi-templated tails, arguing against a primary role of TENT4A/B is poly(A) tail composition in neurons.

Overall, our data suggest that the dynamics of poly(A) tail length that we observed in hippocampal neurons following LTP is mainly related to the transcriptional induction, suggesting that it is mediated by canonical machinery involved in the 3′-end formation. At the same time, we generally observed slightly shorter poly(A) tails in synaptoneurosomes compared to mRNAs from the entire dentate gyrus. This is to be expected since synaptoneurosomes do not contain nascent transcripts that are still present in the nucleus and have the longest tails. Although synaptoneurosomal mRNAs had shorter tails, there was a very small fraction of oligoadenylated mRNAs, which could be re-adenylated in order to drive translation upon stimulation, as proposed for *Camk2a* mRNA. In fact, chemical induction led to the opposite effect: a slight but detectable global poly(A) shortening. As there is growing evidence that deadenylation is a co-translational event, the global activation of translation associated with the deadenylation process explains our observation very well (Bae & Coller, 2022). This is also confirmed by the fact that a large number of mRNAs with shortened poly(A) tails are present in the dentate gyrus 60 min post-HFS. In conclusion, our data do not support cytoplasmic polyadenylation as a mechanism driving translation in hippocampal neurons upon stimulation.

The sequencing data collected allowed us to analyze the alternative polyadenylation site usage, as most mammalian genes possess multiple polyadenylation sites that generate mRNAs with alternative 3′-ends (Elkon et al., 2013). Previous research has demonstrated that *in vitro* LTP, when induced in brain slices, results in widespread shortening of 3′UTRs, consistent with our observation of the general trend of 3'UTR shortening following *in vivo* induced LTP in the rat

hippocampus (Fontes et al., 2017). This indicates a preference for proximal PASs during periods of increased expression, likely due to their greater efficiency compared to distal sites or to circumvent expression suppression by miRNAs (Fontes et al., 2017; Wang et al., 2022).

Finally, studies of the nucleotide composition of poly(A) tails have led us to the discovery of a group of transcripts with semi-templated poly(A) tails. Some of these mRNAs encode proteins that play important roles in synaptic physiology, such as neurogranin (Jones et al., 2018). Since non-adenosine residues inhibit deadenylation, such transcripts may be particularly stable, adding another layer of complexity (Lee et al., 2024). These findings call for further functional analyses to decipher the full spectrum of poly(A) tail-mediated regulation in neuronal physiology. Various stimulation-induced mechanisms leading to changes in mRNA tail length and abundance further illustrate the dynamic nature of mRNA regulation post-HFS.

Methods

Animals

Young adult male Sprague Dawley rats were used (5 months old, 200-300g). They were kept in the laboratory animal facility under a 12-h light/dark cycle with food and water available *ad libitum*. These experimental procedures were approved by Norwegian National Research Ethics Committee in compliance with EU Directive 2010/63/EU, ARRIVE guidelines. Experiments were conducted by the Federation of Laboratory and Animal Science Associations (FELASA) C course-trained and certified researchers.

Stereotaxic surgery and electrode positioning

Rats were anesthetized with 1.5mg/kg of urethane injected intraperitoneally. Once they were unreactive to toe pinch, animals were placed in a stereotaxic frame (David Kopfs Instruments, USA) to fix the head. A thermostatically controlled heating pad was placed under the animal to maintain a temperature of 37°C. The scalp was then cut longitudinally, and the skin held back from the scalp using bulldog clamps. Two burr holes were drilled rostral to bregma to attach the ground and reference screws. For the stimulating electrode, a craniotomy was made on the left hemisphere using bregma as a point of reference (7.9 mm caudal, 4.2 mm lateral, 2.5 mm ventral), these coordinates pinpoint the angular bundle of the medial perforant path. For the recording electrode, a craniotomy was made on the left hemisphere using bregma as a point of reference (3.9 mm caudal, 2.3 mm lateral, ~2.5-3 mm ventral), these coordinates pinpoint the hilar region of the dentate gyrus. The exact depth of the recording electrode was determined when test pulses triggered the maximum fEPSP slope (see next paragraph).

In-vivo electrophysiology

The stimulating electrode sent test pulses every 30 s unilaterally into the medial perforant path in order to evoke field potentials (fEPSPs) in the hilar region of the dentate gyrus which were measured extracellularly using a recording electrode. Stimulus intensities, typically between 100-500 microamps, were set such that they evoked 1/3 of maximum population spike. Baseline potentials were recorded for 24 min. When baseline recordings were completed, the current intensity was doubled and HFS was applied to induce long-term potentiation (LTP). The simulator used was a Grass S88 Dual output stimulator (Grass Medical Instruments, model S88D). The HFS paradigm consisted of three sessions with 5-min intervals totaling 10 min and 30 s. Each session had four trains of 8 pulses delivered at 400 Hz with 10 second intervals between each train. In total there were 96 pulses as previously described (Panja et al., 2014). Post-HFS application, the current was immediately reduced to its test pulse value and the recordings continued at 0.033 Hz for either 10 min or 60 min depending on the experimental group.

Field excitatory postsynaptic potentials (fEPSPs) were recorded using Data Wave Technologies Work Bench Software (Longmont, CO). fEPSP slope was calculated using the maximum positive dV/dt in a selected time window between the fEPSP onset to one-third of the positive peak, based on test-pulse responses during baseline recording. This was done in order to scrutinize only the early EPSPs characteristic of the monosynaptic connection from the entorhinal cortex to the dentate gyrus. Data on the slope and population spike amplitude were transferred to Microsoft Office Excel 2010 (Microsoft Corporation, USA). Every 4 measurements were transformed into a 2-min mean and normalized to the mean of the 24 min of baseline recording. This is to reduce variability and investigate percent change from the average baseline value (average of 4 data points every 30 s so one datapoint is obtained for every 2 min of data). Slope and population spike amplitude averages were analyzed in GraphPad Prism (San Diego, CA), comparing baseline to post-HFS.

Brain dissection

Immediately after the experiment, the rat was removed from the stereotax. For dissection: the brain was removed from the skull and placed on filter paper above a glass plate cooled with ice. Ice-cold saline solution was used periodically through the dissection to cool the brain down. With the hippocampus isolated, blood vessels and connective tissue were removed before the Cornu Ammonis regions were separated from the dentate gyrus and each was put in cold microtubes. The samples were put on dry ice and kept at −80°C. This was done for both the ipsilateral and contralateral dentate gyri.

RNA Extraction and Quality Check

Prior to homogenization tissue was carried on dry ice and then homogenized in 1 mL of Trizol using 1 mL glass/glass dounce homogenizer. Homogenate was transferred to 1.5 ml LoBind® type Eppendorf tube and centrifuged 12000 x g for 5 min in 4°C, due to its high fat content. RNA was then extracted from supernatant using standard manufacturer's protocol. Precipitation was carried out by addition of glycogen (GlycoBlue™ Coprecipitant (15 mg/mL)) (30 µg per sample), 1 volume of isopropanol and overnight incubation in -20°C. RNA pellet was dissolved in RNAse free dd H_2O and preliminary assessed in terms of quality using Nanodrop 2000 Spectrophotometer yielding on average around 20µg of RNA per sample. RNA was then subjected to further purification by precipitation with 3 volumes of KAPA Pure Beads according to manufacturer's instructions (KAPA Biosystems). The assessment of RNA integrity number (RIN) was carried out using the Agilent bioanalyzer (Agilent RNA 6000 Nano Kit). RNA from synaptoneurosomes was isolated using the same method. The amount of Trizol used was approximately 1 mL per 100 mg of synaptoneurosomes pellet.

qRT-PCR

1 µg of RNA samples were reverse transcribed using random primers (GeneON, Ludwigshafen am Rhein, Germany; #S300; 200 ng/RT reaction) and SuperScript IV Reverse Transcriptase (Thermo Fisher Scientific). Next, the cDNA samples were amplified using specific primers (c-fos Fwd: 5'CCCATCCTTACGGACTCCC3'; c-fos Rev: 5'GAGATAGCTGCTCTACTTTGCC3'; Arc Fwd: 5'AAGTGCCGAGCTGAGATGC3'; Arc Rev: 5'CGACCTGTGCAACCCTTTC3'; 18S rRNA Fwd: 5'GTTGGTTTTCGGAACTGAGGC3'; 18S rRNA Rev: 5'GTCGGCATCGTTTATGGTCG3'). Each reaction was set in a final volume of 15 µl, using PowerUp SYBR Green Master Mix (#A25742 Thermo Fisher Scientific) in a LightCycler480 (Roche). Fold changes in expression were determined using the ΔΔ Ct (where Ct is the threshold cycle) relative quantification method. Values were normalized to the relative amounts of 18S rRNA.

Nanopore direct RNA sequencing

The DRS was performed following Bilska et al. (Bilska et al., 2020). For dentate gyri, 4.5-5 µg of total RNA was mixed with 250 ng of oligo(dT)-enriched RNA from *Saccharomyces cerevisiae* and 5 ng of *in vitro* transcribed poly(A) standards. For synaptoneurosomes, 3 µg of cap-enriched RNA was mixed with 200 ng of *S. cerevisiae* oligo(dT)-enriched RNA and 5 ng of poly(A) standards. Libraries were prepared using the Direct RNA Sequencing Kit SQK-RNA002 (ONT). Sequencing utilized FLO-MIN106 R9.4.1 RevD flow cells on a MinION

device controlled by MinKNOW software (ONT). Basecalling was performed with Guppy 6.0.0 (ONT).

Nanopore cDNA sequencing

For dentate gyri, 200 ng of total RNA was used to prepare nanopore cDNA sequencing libraries with the cDNA-PCR Sequencing Kit SQK-PCS111 (ONT) according to the manufacturer's instructions. Sequencing was carried out using FLO-MIN106 R9.4.1 RevD flow cells on a MinION device controlled by MinKNOW software (ONT). The basecalling was performed with Guppy 6.0.0 (ONT) and Dorado 0.5.3 (ONT).

Poly(A) tail length profiling

Basecalled RNA reads were mapped to mRatBN7.2-derived reference transcriptome using minimap2 2.17 (Li, 2018) (-k 14 -ax map-ont --secondary = no) and processed using samtools 1.13 (Danecek et al., 2021) to filter out supplementary alignments and reads mapping to the reverse strand (samtools view -b -F 2320). The lengths of the poly(A) tails were estimated using the Nanopolish 0.13.2 polya function (Workman et al., 2019). Only reads tagged by Nanopolish as PASS or SUFFCLIP were considered in the following analyses.

The lengths of poly(A) tails in cDNA reads were estimated during basecalling with dorado (--estimate-poly-a), extracted from the source files, and aggregated in tabular form.

The NanoTail package (Krawczyk et al., 2024) was used to perform the statistical analysis. The p-values were calculated using the Wilcoxon signed-rank test for transcripts represented by 10 or more reads, and adjustment for multiple comparisons was applied using the Benjamini-Hochberg method. Cohen d was used as an effect size measure. For values $x<0.2$, effect size was considered 'negligible', for values $0.2\leq x<0.5$ it was considered 'small', for values $0.5\leq x<0.8$ it was considered 'medium', and for values $x\geq 0.8$, it was considered 'large'. Transcripts were considered significantly altered in poly(A) tail length if the adjusted p-value was less than 0.05 and the difference in tail length was greater than 5 nt between the hemispheres.

Differential expression

Reads were mapped to the mRatBN7.2 reference genome using minimap2 2.17 (Li, 2018) (-ax splice --secondary = no -uf). The read distribution across genes was summarized using featureCounts from the Subread 2.0.6 package (Liao et al., 2014) (-L --fracOverlap 0.5 --fracOverlapFeature 0.5 -s 1). Reads overlapping multiple features and multimappers were excluded. Differential expression analysis was performed using the DESeq2 (Love et al., 2014) with default settings.

Nucleotide composition of poly(A) tails

Non-adenosine nucleotides in DRS reads were assessed with the Ninetails package (Gumińska et al., 2024). The raw classification results were corrected and further processed as described in Gumińska et al. (Gumińska et al., 2024).

Alternative polyadenylation

The cDNA reads were preprocessed using pychopper 2.7.2 (ONT). Reads fulfilling quality criteria and rescued fused reads were combined, then mapped to the mRatBN7.2 reference genome with minimap2 2.17 (Li, 2018) (-ax splice --secondary = no -uf -k 14). Alternative polyadenylation site analysis was performed with TAPAS (Arefeen et al., 2018) and LAPA (Çelik & Mortazavi, 2022).

Differential usage of poly(A) sites was calculated using two-sided Fisher's exact test. P-values were adjusted using the Benjamini-Hochberg method (given APA site was considered as differentially expressed if adjusted p-value was less or equal to 0.1).

CPEB-binding motif search

CPEB-binding motifs (CPEB-1 and CPEB2-4, respectively) were searched for using the FIMO software (--bgfile --nrdb-- --thresh 1.0E-4) from the MEME suite (Grant et al., 2011). Gene ontology enrichment was performed using g:Profiler (Raudvere et al., 2019) and ClusterProfiler (T. Wu et al., 2021).

Synaptoneurosomes isolation and in vitro stimulation

Synaptoneurosomes were prepared as described previously (Kuzniewska et al., 2018). Before tissue dissection, Krebs buffer (2.5 mM $CaCl_2$, 1.18 mM KH_2PO_4, 118.5 mM NaCl, 24.9 mM $NaHCO_3$, 1.18 mM $MgSO_4$, 3.8 mM $MgCl_2$, and 212.7 mM glucose) was aerated with an aquarium pump for 30 min at 4°C. Next, the pH was lowered to 7.4 using dry ice. The buffer was supplemented with 1× protease inhibitor cocktail complete EDTA-free (Roche) and 60 U/ml RNase Inhibitor (RiboLock, Thermo Fisher Scientific). Animals were euthanized by cervical dislocation; hippocampi were dissected. Tissue from one hemisphere was homogenized in a 1.5 ml Krebs buffer using Dounce homogenizer with 10–12 strokes. All steps were kept ice-cold to prevent the stimulation of synaptoneurosomes. Homogenates were passed gravitationally through a series of presoaked (with Krebs buffer) nylon mesh filters: 100, 60, 30, and 10 µm (Merck Millipore) in cold room to 50-ml polypropylene tube, centrifuged at 1,000 g for 15 min at 4°C, and washed, and pellet was resuspended in Krebs buffer with protease and RNase inhibitors. The protocol for *in vitro* stimulation of NMDA receptors on

synaptoneurosomes was described before (Kuzniewska et al 2018). The aliquots of freshly isolated synaptoneurosomes were prewarmed for 5 min at 37°C and stimulated with a pulse of 50 μM NMDA and 10 μM glutamate for 30 s; then, APV (120 μM) was added and synaptoneurosomes were further incubated for 10 min at 37°C. Unstimulated samples, kept on ice, were used as controls. Synaptoneurosomes isolated from 5 rats were pooled together and split into two samples (control and NMDAR-stimulated) in order to obtain enough material for Nanopore Direct RNA Sequencing (DRS). Four independent synaptoneurosomes isolations were used for DRS.

Western blotting analysis of synaptoneurosomal preparations

Equal amounts of protein from homogenate and synaptoneurosomal fraction were resolved on SDS-PAGE (10%, TGX Stain-Free FastCast Acrylamide Solutions, BioRad). After electrophoresis proteins in the gel were visualized using Bio-Rad's ImageLab software to verify the equal protein loading. Proteins were transferred to PVDF membranes (pore size 0.45 μm, Immobilon-P, Merck Millipore) using Trans-Blot Turbo Blotting System (BioRad; 170-4155). Membranes were blocked for 1 h at room temperature in 5% non-fat dry milk in PBS-T (PBS with 0.01% Tween-20), followed by overnight incubation at 4°C with primary antibodies (synaptophysin Cat#MAB329, Merck Millipore; GluA2 Cat#13607, Cell Signaling; Psd95 Cat#MAB1598, Merck Millipore; Gfap Cat#16825-1-AP; Proteintech; tubulin Cat#sc-134239, Santa Cruz Biotechnology; Hsp90 Cat#ab13495, Abcam; Kdm1 Cat#ab129195, Abcam; c-Jun Cat#9165, Cell Signaling) in 5% milk in PBS-T. Blots were washed 3 × 5 min with PBS-T, incubated 1 h at room temperature with HRP-conjugated secondary antibody (1:10 000 in 5% milk) and washed 3 × 5 min with PBS-T. In the case of MAPK/Phospho-MAPK Family Antibody Sampler Kit, membranes were blocked for 1 h at room temperature in 5% bovine serum albumin (BSA) in PBS-T, primary and secondary antibodies were diluted also in 5% BSA in PBS-T. HRP signal was detected using Amersham ECL Prime Western Blotting Detection Reagent (GE Healthcare) on ChemiDoc Imaging System (BioRad) using automatic detection settings.

Data visualization

The visualization of the data was performed in the R environment. Poly(A) nucleotide composition analyses using Ninetails (Gumińska et al., 2024). Heatmaps were created with ComplexHeatmap (Gu, 2022), and genome browser-like diagrams were drawn using ggcoverage (Song & Wang, 2023). The remaining diagrams were created using ggplot2 (Wickham, 2016).

Acknowledgements

We would like to thank all the lab members of our collaborating groups for their support and fruitful discussions. The research leading to these results was funded by the Norwegian Financial Mechanism 2014 -2021, no. UMO-2019/34/H/NZ3/00733.

Author contributions

NG supervised by PK performed all the bioinformatic analyses and prepared figure drafts; FPP supported by PUG performed *in vivo* LTP. BK, PW and JM analyzed RNA samples and performed experiments on synaptoneurosomes. SM and SJ were responsible for nanopore sequencing. NG, FPP, AD, and MD wrote the manuscript. CRB, AD, and MD jointly supervised and directed the studies.

Supplementary data

Supplementary Figures are provided in attached .pdf file.

Supplementary Tables are deposited in Zenodo: https://doi.org/10.5281/zenodo.11478468

Raw sequencing data (fast5 files) are deposited at the European Nucleotide Archive (ENA) (https://www.ebi.ac.uk/ena/browser/home) under the project numbers (PRJEB75352 and PRJEB75356) with sample numbers listed in Supplementary Table 6. Source data used for plotting are provided in Supplementary Tables 1-5.

Custom software (NanoTail) used for poly(A) tail analysis in R is available here: https://github.com/LRB-IIMCB/nanotail.

Custom software (Ninetails) used for non-adenosine profiling is available here: https://github.com/LRB-IIMCB/ninetails.

References

Arefeen, A., Liu, J., Xiao, X., & Jiang, T. (2018). TAPAS: Tool for alternative polyadenylation site analysis. *Bioinformatics (Oxford, England)*, *34*(15), 2521–2529. https://doi.org/10.1093/bioinformatics/bty110

Arora, A., Goering, R., Lo, H. Y. G., Lo, J., Moffatt, C., & Taliaferro, J. M. (2021). The Role of Alternative Polyadenylation in the Regulation of Subcellular RNA Localization. *Frontiers in Genetics*, *12*, 818668. https://doi.org/10.3389/fgene.2021.818668

Bae, H., & Coller, J. (2022). Codon optimality-mediated mRNA degradation: Linking translational elongation to mRNA stability. *Molecular Cell*, *82*(8), 1467–1476. https://doi.org/10.1016/j.molcel.2022.03.032

Bilska, A., Kusio-Kobiałka, M., Krawczyk, P. S., Gewartowska, O., Tarkowski, B., Kobyłecki, K., Nowis, D., Golab, J., Gruchota, J., Borsuk, E., Dziembowski, A., & Mroczek, S. (2020). Immunoglobulin expression and the humoral immune response is regulated by the non-canonical poly(A) polymerase TENT5C. *Nature Communications*, *11*(1). https://doi.org/10.1038/S41467-020-15835-3

Bramham, C. R., Jensen, K. B., & Proud, C. G. (2016). Tuning Specific Translation in Cancer Metastasis and Synaptic Memory: Control at the MNK-eIF4E Axis. *Trends in Biochemical Sciences*, *41*(10), 847–858. https://doi.org/10.1016/j.tibs.2016.07.008

Bramham, C. R., & Wells, D. G. (2007). Dendritic mRNA: Transport, translation and function. *Nature Reviews. Neuroscience*, *8*(10), 776–789. https://doi.org/10.1038/nrn2150

Brouze, A., Krawczyk, P. S., Dziembowski, A., & Mroczek, S. (2023). Measuring the tail: Methods for poly(A) tail profiling. *Wiley Interdisciplinary Reviews: RNA*, *14*(1), e1737. https://doi.org/10.1002/WRNA.1737

Cagnetta, R., Flanagan, J. G., & Sonenberg, N. (2023). Control of Selective mRNA Translation in Neuronal Subcellular Compartments in Health and Disease. *The Journal of Neuroscience: The Official Journal of the Society for Neuroscience*, *43*(44), 7247–7263. https://doi.org/10.1523/JNEUROSCI.2240-22.2023

Çelik, M. H., & Mortazavi, A. (2022). *Analysis of alternative polyadenylation from long-read or short-read RNA-seq with LAPA* (p. 2022.11.08.515683). bioRxiv. https://doi.org/10.1101/2022.11.08.515683

Chang, H., Lim, J., Ha, M., & Kim, V. N. (2014). TAIL-seq: Genome-wide determination of poly(A) tail length and 3' end modifications. *Molecular Cell*, *53*(6), 1044–1052. https://doi.org/10.1016/J.MOLCEL.2014.02.007

Chen, P. B., Kawaguchi, R., Blum, C., Achiro, J. M., Coppola, G., O'Dell, T. J., & Martin, K. C. (2017). Mapping Gene Expression in Excitatory Neurons during Hippocampal Late-Phase Long-Term Potentiation. *Frontiers in Molecular Neuroscience*, *10*, 39. https://doi.org/10.3389/fnmol.2017.00039

Citri, A., & Malenka, R. C. (2008). Synaptic plasticity: Multiple forms, functions, and mechanisms. *Neuropsychopharmacology: Official Publication of the American College of Neuropsychopharmacology*, *33*(1), 18–41. https://doi.org/10.1038/sj.npp.1301559

Colgan, D. F., & Manley, J. L. (1997). Mechanism and regulation of mRNA polyadenylation. *Genes & Development*, *11*(21), 2755–2766. https://doi.org/10.1101/gad.11.21.2755

Danecek, P., Bonfield, J. K., Liddle, J., Marshall, J., Ohan, V., Pollard, M. O., Whitwham, A., Keane, T., McCarthy, S. A., Davies, R. M., & Li, H. (2021). Twelve years of SAMtools and BCFtools. *GigaScience*, *10*(2), giab008. https://doi.org/10.1093/gigascience/giab008

de Moor, C. H., & Richter, J. D. (1999). Cytoplasmic polyadenylation elements mediate masking and unmasking of cyclin B1 mRNA. *The EMBO Journal*, *18*(8), 2294–2303. https://doi.org/10.1093/emboj/18.8.2294

Demmer, J., Dragunow, M., Lawlor, P. A., Mason, S. E., Leah, J. D., Abraham, W. C., & Tate, W. P. (1993). Differential expression of immediate early genes after hippocampal long-term potentiation in awake rats. *Brain Research. Molecular Brain Research*, *17*(3–4), 279–286. https://doi.org/10.1016/0169-328x(93)90012-e

Di Giammartino, D. C., Nishida, K., & Manley, J. L. (2011). Mechanisms and consequences of alternative polyadenylation. *Molecular Cell*, *43*(6), 853–866. https://doi.org/10.1016/j.molcel.2011.08.017

Du, L., & Richter, J. D. (2005). Activity-dependent polyadenylation in neurons. *RNA (New York, N.Y.)*, *11*(9), 1340–1347. https://doi.org/10.1261/rna.2870505

Eisen, T. J., Eichhorn, S. W., Subtelny, A. O., Lin, K. S., McGeary, S. E., Gupta, S., & Bartel, D. P. (2020). The Dynamics of Cytoplasmic mRNA Metabolism. *Molecular Cell*, *77*(4), 786-799.e10. https://doi.org/10.1016/j.molcel.2019.12.005

Eisen, T. J., Li, J. J., & Bartel, D. P. (2022). The interplay between translational efficiency, poly(A) tails, microRNAs, and neuronal activation. *RNA*, *28*(6), 808–831. https://doi.org/10.1261/rna.079046.121

Elkon, R., Ugalde, A. P., & Agami, R. (2013). Alternative cleavage and polyadenylation: Extent, regulation and function. *Nature Reviews. Genetics*, *14*(7), 496–506. https://doi.org/10.1038/nrg3482

Fontes, M. M., Guvenek, A., Kawaguchi, R., Zheng, D., Huang, A., Ho, V. M., Chen, P. B., Liu, X., O'Dell, T. J., Coppola, G., Tian, B., & Martin, K. C. (2017). Activity-Dependent Regulation of Alternative Cleavage and Polyadenylation During Hippocampal Long-Term Potentiation. *Scientific Reports*, *7*(1), 17377. https://doi.org/10.1038/s41598-017-17407-w

Grant, C. E., Bailey, T. L., & Noble, W. S. (2011). FIMO: Scanning for occurrences of a given motif. *Bioinformatics*, *27*(7), 1017–1018. https://doi.org/10.1093/bioinformatics/btr064

Gu, Z. (2022). Complex heatmap visualization. *iMeta*, *1*(3), e43. https://doi.org/10.1002/IMT2.43

Gumińska, N., Matylla-Kulińska, K., Krawczyk, P. S., Maj, M., Orzeł, W., Mackiewicz, Z., Brouze, A., Mroczek, S., & Dziembowski, A. (2024). *Direct profiling of non-adenosines in poly(A) tails of endogenous and therapeutic mRNAs with Ninetails*.

Guzowski, J. F., McNaughton, B. L., Barnes, C. A., & Worley, P. F. (1999). Environment-specific expression of the immediate-early gene Arc in hippocampal neuronal ensembles. *Nature Neuroscience*, *2*(12), 1120–1124. https://doi.org/10.1038/16046

Ha, K. C. H., Sterne-Weiler, T., Morris, Q., Weatheritt, R. J., & Blencowe, B. J. (2021). Differential contribution of transcriptomic regulatory layers in the definition of neuronal identity. *Nature Communications*, *12*(1), 335. https://doi.org/10.1038/s41467-020-20483-8

Hoque, M., Ji, Z., Zheng, D., Luo, W., Li, W., You, B., Park, J. Y., Yehia, G., & Tian, B. (2013). Analysis of alternative cleavage and polyadenylation by 3' region extraction and deep sequencing. *Nature Methods*, *10*(2), 133–139. https://doi.org/10.1038/nmeth.2288

Huang, Y.-S., Mendez, R., Fernandez, M., & Richter, J. D. (2023). CPEB and translational control by cytoplasmic polyadenylation: Impact on synaptic plasticity, learning, and memory. *Molecular Psychiatry*, *28*(7), 2728–2736. https://doi.org/10.1038/s41380-023-02088-x

Jasińska, M., Miłek, J., Cymerman, I. A., Łęski, S., Kaczmarek, L., & Dziembowska, M. (2016). miR-132 Regulates Dendritic Spine Structure by Direct Targeting of Matrix Metalloproteinase 9 mRNA. *Molecular Neurobiology*, *53*(7), 4701–4712. https://doi.org/10.1007/s12035-015-9383-z

Jones, K. J., Templet, S., Zemoura, K., Kuzniewska, B., Pena, F. X., Hwang, H., Lei, D. J., Haensgen, H., Nguyen, S., Saenz, C., Lewis, M., Dziembowska, M., & Xu, W. (2018). Rapid, experience-dependent translation of neurogranin enables memory encoding. *Proceedings of the National Academy of Sciences of the United States of America*, *115*(25), E5805–E5814. https://doi.org/10.1073/pnas.1716750115

Kim, S., Kim, H., & Um, J. W. (2018). Synapse development organized by neuronal activity-regulated immediate-early genes. *Experimental & Molecular Medicine*, *50*(4), 1–7. https://doi.org/10.1038/s12276-018-0025-1

Krause, M., Niazi, A. M., Labun, K., Torres Cleuren, Y. N., Müller, F. S., & Valen, E. (2019). tailfindr: Alignment-free poly(A) length measurement for Oxford Nanopore RNA and DNA sequencing. *RNA*, *25*(10), 1229–1241. https://doi.org/10.1261/rna.071332.119

Krawczyk, P. S., Tudek, A., Mroczek, S., & Dziembowski, A. (2024). Transcriptome-Wide Analysis of mRNA Adenylation Status in Yeast Using Nanopore Sequencing. *Methods*

in Molecular Biology (Clifton, N.J.), *2723*, 193–214. https://doi.org/10.1007/978-1-0716-3481-3_12

Kuzniewska, B., Chojnacka, M., Milek, J., & Dziembowska, M. (2018). Preparation of polysomal fractions from mouse brain synaptoneurosomes and analysis of polysomal-bound mRNAs. *Journal of Neuroscience Methods*, *293*, 226–233. https://doi.org/10.1016/j.jneumeth.2017.10.006

Kuzniewska, B., Cysewski, D., Wasilewski, M., Sakowska, P., Milek, J., Kulinski, T. M., Winiarski, M., Kozielewicz, P., Knapska, E., Dadlez, M., Chacinska, A., Dziembowski, A., & Dziembowska, M. (2020). Mitochondrial protein biogenesis in the synapse is supported by local translation. *EMBO Reports*, *21*(8), e48882. https://doi.org/10.15252/embr.201948882

Lau, A. G., Irier, H. A., Gu, J., Tian, D., Ku, L., Liu, G., Xia, M., Fritsch, B., Zheng, J. Q., Dingledine, R., Xu, B., Lu, B., & Feng, Y. (2010). Distinct 3'UTRs differentially regulate activity-dependent translation of brain-derived neurotrophic factor (BDNF). *Proceedings of the National Academy of Sciences of the United States of America*, *107*(36), 15945–15950. https://doi.org/10.1073/pnas.1002929107

Lee, Y., Levdansky, Y., Jung, Y., Kim, V. N., & Valkov, E. (2024). Deadenylation kinetics of mixed poly(A) tails at single-nucleotide resolution. *Nature Structural & Molecular Biology*, 1–9. https://doi.org/10.1038/s41594-023-01187-1

Legnini, I., Alles, J., Karaiskos, N., Ayoub, S., & Rajewsky, N. (2019). FLAM-seq: Full-length mRNA sequencing reveals principles of poly(A) tail length control. *Nature Methods 2019 16:9*, *16*(9), 879–886. https://doi.org/10.1038/s41592-019-0503-y

Li, H. (2018). Minimap2: Pairwise alignment for nucleotide sequences. *Bioinformatics*, *34*(18), 3094–3100. https://doi.org/10.1093/bioinformatics/bty191

Liao, Y., Smyth, G. K., & Shi, W. (2014). featureCounts: An efficient general purpose program for assigning sequence reads to genomic features. *Bioinformatics (Oxford, England)*, *30*(7), 923–930. https://doi.org/10.1093/bioinformatics/btt656

Lim, J., Kim, D., Lee, Y.-S., Ha, M., Lee, M., Yeo, J., Chang, H., Song, J., Ahn, K., & Kim, V. N. (2018). Mixed tailing by TENT4A and TENT4B shields mRNA from rapid deadenylation. *Science (New York, N.Y.)*, *361*(6403), 701–704. https://doi.org/10.1126/science.aam5794

Liu, Y., Nie, H., Liu, H., & Lu, F. (2019). Poly(A) inclusive RNA isoform sequencing (PAIso-seq) reveals wide-spread non-adenosine residues within RNA poly(A) tails. *Nature Communications*, *10*(1). https://doi.org/10.1038/S41467-019-13228-9

Love, M. I., Huber, W., & Anders, S. (2014). Moderated estimation of fold change and dispersion for RNA-seq data with DESeq2. *Genome Biology*, *15*(12), 550. https://doi.org/10.1186/s13059-014-0550-8

Maag, J. L. V., Panja, D., Sporild, I., Patil, S., Kaczorowski, D. C., Bramham, C. R., Dinger, M. E., & Wibrand, K. (2015). Dynamic expression of long noncoding RNAs and repeat elements in synaptic plasticity. *Frontiers in Neuroscience*, *9*, 351. https://doi.org/10.3389/fnins.2015.00351

Mansur, F., Alarcon, J. M., Stackpole, E. E., Wang, R., & Richter, J. D. (2021). Noncanonical cytoplasmic poly(A) polymerases regulate RNA levels, alternative RNA processing, and synaptic plasticity but not hippocampal-dependent behaviours. *RNA Biology*, *18*(7), 962–971. https://doi.org/10.1080/15476286.2020.1824061

Mansur, F., Ivshina, M., Gu, W., Schaevitz, L., Stackpole, E., Gujja, S., Edwards, Y. J. K., & Richter, J. D. (2016). Gld2-catalyzed 3' monoadenylation of miRNAs in the hippocampus has no detectable effect on their stability or on animal behavior. *RNA (New York, N.Y.)*, *22*(10), 1492–1499. https://doi.org/10.1261/rna.056937.116

Mauxion, F., Faux, C., & Séraphin, B. (2008). The BTG2 protein is a general activator of mRNA deadenylation. *The EMBO Journal*, *27*(7), 1039–1048. https://doi.org/10.1038/emboj.2008.43

McFleder, R. L., Mansur, F., & Richter, J. D. (2017). Dynamic Control of Dendritic mRNA Expression by CNOT7 Regulates Synaptic Efficacy and Higher Cognitive Function. *Cell Reports*, *20*(3), 683–696. https://doi.org/10.1016/j.celrep.2017.06.078

Miura, P., Shenker, S., Andreu-Agullo, C., Westholm, J. O., & Lai, E. C. (2013). Widespread and extensive lengthening of 3' UTRs in the mammalian brain. *Genome Research*, *23*(5), 812–825. https://doi.org/10.1101/gr.146886.112

Panja, D., Kenney, J. W., D'Andrea, L., Zalfa, F., Vedeler, A., Wibrand, K., Fukunaga, R., Bagni, C., Proud, C. G., & Bramham, C. R. (2014). Two-stage translational control of dentate gyrus LTP consolidation is mediated by sustained BDNF-TrkB signaling to MNK. *Cell Reports*, *9*(4), 1430–1445. https://doi.org/10.1016/j.celrep.2014.10.016

Pardo-Palacios, F. J., Wang, D., Reese, F., Diekhans, M., Carbonell-Sala, S., Williams, B., Loveland, J. E., De María, M., Adams, M. S., Balderrama-Gutierrez, G., Behera, A. K., Gonzalez, J. M., Hunt, T., Lagarde, J., Liang, C. E., Li, H., Jerryd Meade, M., Moraga Amador, D. A., Prjibelski, A. D., … Brooks, A. N. (2023). Systematic assessment of long-read RNA-seq methods for transcript identification and quantification. *bioRxiv*, 2023.07.25.550582. https://doi.org/10.1101/2023.07.25.550582

Patil, S., Chalkiadaki, K., Mergiya, T. F., Krimbacher, K., Amorim, I. S., Akerkar, S., Gkogkas, C. G., & Bramham, C. R. (2023). eIF4E phosphorylation recruits β-catenin to mRNA cap and promotes Wnt pathway translation in dentate gyrus LTP maintenance. *iScience*, *26*(5), 106649. https://doi.org/10.1016/j.isci.2023.106649

Raudvere, U., Kolberg, L., Kuzmin, I., Arak, T., Adler, P., Peterson, H., & Vilo, J. (2019). g:Profiler: A web server for functional enrichment analysis and conversions of gene lists (2019 update). *Nucleic Acids Research*, *47*(W1), W191–W198. https://doi.org/10.1093/nar/gkz369

Richter, J. D. (2007). CPEB: A life in translation. *Trends in Biochemical Sciences*, *32*(6), 279–285. https://doi.org/10.1016/j.tibs.2007.04.004

Sessegolo, C., Cruaud, C., Da Silva, C., Cologne, A., Dubarry, M., Derrien, T., Lacroix, V., & Aury, J.-M. (2019). Transcriptome profiling of mouse samples using nanopore sequencing of cDNA and RNA molecules. *Scientific Reports*, *9*(1), 14908. https://doi.org/10.1038/s41598-019-51470-9

Song, Y., & Wang, J. (2023). ggcoverage: An R package to visualize and annotate genome coverage for various NGS data. *BMC Bioinformatics*, *24*(1), 309. https://doi.org/10.1186/s12859-023-05438-2

Subtelny, A. O., Eichhorn, S. W., Chen, G. R., Sive, H., & Bartel, D. P. (2014). Poly(A)-tail profiling reveals an embryonic switch in translational control. *Nature*, *508*(7494), 66–71. https://doi.org/10.1038/nature13007

Thomas, K. T., Gross, C., & Bassell, G. J. (2018). microRNAs Sculpt Neuronal Communication in a Tight Balance That Is Lost in Neurological Disease. *Frontiers in Molecular Neuroscience*, *11*, 455. https://doi.org/10.3389/fnmol.2018.00455

Tushev, G., Glock, C., Heumüller, M., Biever, A., Jovanovic, M., & Schuman, E. M. (2018). Alternative 3' UTRs Modify the Localization, Regulatory Potential, Stability, and Plasticity of mRNAs in Neuronal Compartments. *Neuron*, *98*(3), 495-511.e6. https://doi.org/10.1016/j.neuron.2018.03.030

Udagawa, T., Swanger, S. A., Takeuchi, K., Kim, J. H., Nalavadi, V., Shin, J., Lorenz, L. J., Zukin, R. S., Bassell, G. J., & Richter, J. D. (2012). Bidirectional control of mRNA translation and synaptic plasticity by the cytoplasmic polyadenylation complex. *Molecular Cell*, *47*(2), 253–266. https://doi.org/10.1016/j.molcel.2012.05.016

Wang, J., Chen, W., Yue, W., Hou, W., Rao, F., Zhong, H., Qi, Y., Hong, N., Ni, T., & Jin, W. (2022). Comprehensive mapping of alternative polyadenylation site usage and its dynamics at single-cell resolution. *Proceedings of the National Academy of Sciences of*

the United States of America, *119*(49), e2113504119. https://doi.org/10.1073/pnas.2113504119

Warkocki, Z., Liudkovska, V., Gewartowska, O., Mroczek, S., & Dziembowski, A. (2018). Terminal nucleotidyl transferases (TENTs) in mammalian RNA metabolism. *Philosophical Transactions of the Royal Society of London. Series B, Biological Sciences*, *373*(1762), 20180162. https://doi.org/10.1098/rstb.2018.0162

Wen, X., Irshad, A., & Jin, H. (2023). The Battle for Survival: The Role of RNA Non-Canonical Tails in the Virus-Host Interaction. *Metabolites*, *13*(9), 1009. https://doi.org/10.3390/metabo13091009

Wickham, H. (2016). *ggplot2: Elegant Graphics for Data Analysis* (2nd ed. 2016 edition). Springer.

Wongsurawat, T., Jenjaroenpun, P., Wanchai, V., & Nookaew, I. (2022). Native RNA or cDNA Sequencing for Transcriptomic Analysis: A Case Study on Saccharomyces cerevisiae. *Frontiers in Bioengineering and Biotechnology*, *10*, 842299. https://doi.org/10.3389/fbioe.2022.842299

Workman, R. E., Tang, A. D., Tang, P. S., Jain, M., Tyson, J. R., Razaghi, R., Zuzarte, P. C., Gilpatrick, T., Payne, A., Quick, J., Sadowski, N., Holmes, N., de Jesus, J. G., Jones, K. L., Soulette, C. M., Snutch, T. P., Loman, N., Paten, B., Loose, M., … Timp, W. (2019). Nanopore native RNA sequencing of a human poly(A) transcriptome. *Nature Methods*, *16*(12), 1297–1305. https://doi.org/10.1038/S41592-019-0617-2

Wu, L., Wells, D., Tay, J., Mendis, D., Abbott, M. A., Barnitt, A., Quinlan, E., Heynen, A., Fallon, J. R., & Richter, J. D. (1998). CPEB-mediated cytoplasmic polyadenylation and the regulation of experience-dependent translation of alpha-CaMKII mRNA at synapses. *Neuron*, *21*(5), 1129–1139. https://doi.org/10.1016/s0896-6273(00)80630-3

Wu, T., Hu, E., Xu, S., Chen, M., Guo, P., Dai, Z., Feng, T., Zhou, L., Tang, W., Zhan, L., Fu, X., Liu, S., Bo, X., & Yu, G. (2021). clusterProfiler 4.0: A universal enrichment tool for interpreting omics data. *Innovation (Cambridge (Mass.))*, *2*(3), 100141. https://doi.org/10.1016/j.xinn.2021.100141

Yu, S., & Kim, V. N. (2020). A tale of non-canonical tails: Gene regulation by post-transcriptional RNA tailing. *Nature Reviews Molecular Cell Biology 2020 21:9*, *21*(9), 542–556. https://doi.org/10.1038/s41580-020-0246-8